*Int. J. Electrochem. Sci.*, 16 **(2021)** Article ID: 21094, doi: 10.20964/2021.09.22

International Journal of
ELECTROCHEMICAL
SCIENCE
www.electrochemsci.org

# Phosphorylated NiCo Metal–Organic-Frameworks for Efficient Oxygen Evolution Reaction

*Meng Zong*[1,#,*], *Keke Wang*[2,3,#], *Zongshan Lin*[2,3] *and Zhenghua Tang*[2*]

[1] Chongqing Chemical Industry Vocational College, Chongqing, 401220, China.
[2] Guangzhou Key Laboratory for Surface Chemistry of Energy Materials and New Energy Research Institute, School of Environment and Energy, South China University of Technology, Guangzhou Higher Education Mega Centre, Guangzhou, 510006, China.
[3] School of Pharmacy, Guangdong Pharmaceutical University, Guangzhou, 510006, China.
[*]E-mail: ahzmeng@126.com , zhht@scut.edu.cn
[#]These authors contributed equally.

*Received:* 1 xxx 2021 / *Accepted:* 16 June 2021 / *Published:* 10 August 2021

The development of abundant-element-based, cost-effective, and efficient catalysts for oxygen evolution reaction (OER) holds great promises to realize the practical water splitting. Herein, we report a facile phosphorylation treatment to boost the OER performance of NiCo metal organic frameworks (MOFs). Compared with the parent hollow bowl-like sphere NiCo-MOF, the optimal NiCo-MOF/$Co_2P_2O_7$ had a lower overpotential of 408 mV at 50 mA $cm^{-2}$ and 583 mV at 200 mA $cm^{-2}$. The MOF/$Co_2P_2O_7$ sample also demonstrated markedly superior long term durability for OER to the benchmark $RuO_2$ catalyst. Such excellent performance can be attributed to the well-defined porous structure imparted enhanced reaction kinetics, the formation of phosphates with high oxygen content, and the synergistic catalytic effects of between Ni and Co. The findings here offer a new way in developing high-efficiency and durable MOF-based electrocatalysts for water splitting and beyond.

**Keywords:** Phosphorous treatment; NiCo alloy; Metal organic frameworks; Oxygen evolution reaction, Long term durability

## 1. INTRODUCTION

Electrochemical water splitting to produce $H_2$ and $O_2$ has been extensively regarded as one promising technology to provide a clean and renewable energy sources.[1, 2] Two reactions are involved in this process, one is the hydrogen evolution reaction (HER), the other is the oxygen evolution reaction (OER). Compared to HER, OER is the more dominant limiting process to realize industrial water splitting, as larger overpotential is required to drive the OER reaction to complete the 4-electron transfer

path and covalent O-O bond formation.[3] State-of-the-art catalysts for OER are typically the precious metal-based compounds, such as $IrO_2$, $RuO_2$.[4] However, their large-scale commercialization are significantly restricted by the low natural abundance and high costs. To that end, developing cost effective, efficient, abundant-elements-based OER catalysts is highly desirable.[5]

Recently, transition-metal-based materials including transition metal hydroxides,[6] oxides,[7] sulfides,[8] selenides[9], phosphide,[10] and transition metal composites[11, 12] have been garnering continuous increasing research attentions as alternative OER catalysts, thanks to their easy availability, low-cost, excellent activity, and environmental friendliness. Metal organic frameworks (MOFs) have been widely employed to prepare transition-metal-based OER catalysts. It is well-known that, upon high-temperature thermal treatment and pyrolysis, MOFs can turn into porous carbon materials with high surface area, good conductivity, and even more importantly, the rich and well-defined porous structure of such porous carbon can be beneficial for the electron and mass transfer behaviors for the electrocatalytic reactions.[13-15] However, the high-temperature thermal treatment and pyrolysis normally destroy the intrinsic well-defined structure of MOFs, neither not environmental friendly, nor obscuring the eventual structure-activity relationship establishment for the fundamental study. To that end, more and more research efforts have been switched to developing MOFs based OER catalysts rather than MOFs-derived catalysts.[16] For instance, Li group prepared missing-linker MOFs of CoBDC, of which the array exhibited outstanding OER performance with rather low overpotential of 241 mV at the current density of 100 mA $cm^{-2}$.[17] The enhancement of the OER performance is likely due to that, the introduction of the missing likers fine-tuned the electronic structure of the CoBDC. In another study, Yan and colleagues designed a rational linker scission approach to induce lattice strain to prepare strained NiFe-MOFs with 6% lattice expansion, which showed a superior OER performance with overpotential of 230 mV at 10 mA $cm^{-2}$ and long-term catalytic stability.[18] Despite the above progresses, the studies of directly using MOFs for OER are still rare, and further boosting the OER performance has becoming a long pursuing goal in the relevant research community.

Inspired by the above investigations, herein, we report a novel type phosphorylated NiCo MOFs for OER by solvothermal synthesis, in which NiCo-MOF is a hollow bowl-like sphere assembled by nanosheets. The OER performance of NiCo-MOF was drastically enhanced by the phosphorylation treatment. The resultant NiCo-MOF/$Co_2P_2O_7$ exhibited improved OER performance to NiCo-MOF, as the lower overpotential of 408 mV @ 50 mA $cm^{-2}$ than that of NiCo-MOF (442 mV). NiCo-MOF/$Co_2P_2O_7$ also possessed a small Tafel slope of 106.4 mV $dec^{-1}$. Such NiCo-MOF/$Co_2P_2O_7$ catalyst also possessed remarkably outperformed long-term durability to the $RuO_2$ benchmark. The novelty of this work includes two points: 1. Instead of using pyrolyzed MOF to fabricate porous carbon material for electrocatalysis, direct utilizing MOF as electrocatalyst not only can preserve the well-defined structure of MOF, but also is environmentally friendly with much lower energy required; 2. A quite facile and straightforward phosphorylation method is developed here to enhance the OER performance for MOF, which has been rarely reported in previous studies.

## 2. MATERIALS AND METHODS

### *2.1. Reagents and Materials*

Cobaltous (II) nitrate hexahydrate (Co $(NO_3)_2 \cdot 6H_2O$, ≥98.0%), nickel (II) nitrate hexahydrate (Ni $(NO_3)_2 \cdot 6H_2O$, ≥99.5%), ammonium dihydrogen phosphate ($NH_4H_2PO_4$), terephthalic acid (1,4-$H_2BDC$), N, N-dimethylacetamide (DMAC), N, N-dimethylformamide (DMF), isopropanol and absolute ethanol (≥99.5%), the Nafion solution (5 wt. %) were bought from Damao Chemical Reagents (Tianjin, China). Commercial ruthenium dioxide ($RuO_2$, 99.9% metal basis) was purchased from Aladdin (Shanghai, China). The deionized water (resistivity is 18.3 $M\Omega \cdot cm^{-1}$) was prepared by a Barnstead water purification system and used throughout the study. All reagents were used as received without further purification.

### *2.2. Preparation of the NiCo-MOF hollow bowl-shaped nanosphere*

The hollow bowl-shaped nanosphere of NiCo-based metal organic framework (abbreviated as NiCo-MOF) was fabricated by following the documented procedure with some modifications.[19] Briefly, a DMAC solution of 1, 4-$H_2BDC$ (41.5 mg, 0.25 mmol in 12.5 mL), a total amount of 0.75 mmol of $Ni(NO_3)_2 \cdot 6H_2O$ and $Co(NO_3)_2 \cdot 6H_2O$ with various Ni/Co ratios in 25 mL DMAC solution were mixed and 22.5 mL isopropanol was added to a 100 mL Teflon vessel subsequently. After shaking for a few mins, the container was transferred in a stainless-steel autoclave and heated in an oven at 150 °C for 3 h, and subsequently naturally cooled down to room temperature. After that, the precipitates were collected by centrifugation at 8000 rpm and washed with water and ethanol 3 times prior to drying at 60 °C for 12 h.

### *2.3. Synthesis of the NiCo-MOF/$Co_2P_2O_7$ catalyst*

In a typical synthesis,[20] firstly, 30 mg freshly-prepared NiCo-MOF hollow bowl-shaped nanosphere was dispersed in a mixed solvent (24 mL) with a volume ratio of $V_{DMF}$: $V_{H2O}$ = 7: 1 under constant stirring. Then, 4.0 mmol of Co $(NO_3)_2 \cdot 6H_2O$ and x mmol of $NH_4H_2PO_4$ were introduced. After continuous stirring about 5 mins, the mixed solution was transferred into a 50 mL Teflon autoclave for solvothermal reaction at 100 ℃ with 5 h. The product was subsequently collected by centrifugation at 8000 rpm for 5 min, and washed with a mixed solvent of absolute ethanol and water for several times. Finally, the product was dried in vacuum at 60 °C for 12 h, and it is named as NiCo-MOF/$Co_2P_2O_7$.

### *2.4. Characterization*

The surface microstructures of the samples were examined via field emission scanning electron microscopy (SEM, Hitachi S-4800) and transmission electron microscopy (TEM, Tecnai G2 F30). The X-ray diffraction (XRD) patterns in the Bragg's angle range (2θ) of 10°-90° were collected using a Bruker D8 diffractometer with Cu $K_\alpha$ ($\lambda$ = 0.1541 nm) radiation.

*2.5. Electrochemical measurements*

Electrochemical measurements were conducted with a CHI electrochemical workstation (750E, CHI Instruments Inc, USA) in 1 M KOH aqueous solution at room temperature without iR-compensation. A three-electrode system was utilized in the OER test, of which Ag/AgCl was chosen as the reference electrode, while the carbon rod and the carbon cloth electrode were utilized as the counter electrode and the working electrode, respectively. The catalyst ink was prepared as follows: 5 mg of the catalyst was dispersed in 500 μL of absolute ethanol with the aid of ultrasonication, following by the sequential addition of 450 μL of nanopure water and 50 μL of Nafion to form a uniform suspension. 20 μL of the suspension was dropwise cast onto a single-sided carbon cloth (1 cm x 0.5 cm, load area is 0.5 $cm^2$), and dried at room temperature. The catalyst loading was estimated as ~200 μg $cm^{-2}$. The solution was saturated with nitrogen at least 30 mins prior to each measurement.

## 3. RESULTS AND DISCUSSION

*3.1. Synthesis and characterization*

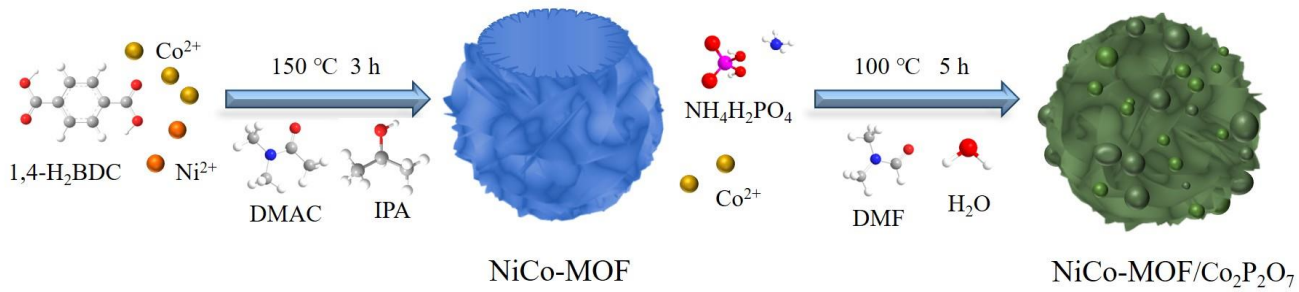


**Scheme 1** The schematic illustration of the synthetic route to NiCo-MOF/$Co_2P_2O_7$.

As illustrated in Scheme 1, the NiCo-MOF/$Co_2P_2O_7$ catalyst was prepared through a two-step reaction process. Firstly, the NiCo-MOF hollow bowl-shaped nanosphere was readily synthesized by a solvothermal reaction of 1, 4-$H_2$BDC, Ni $(NO_3)_2 \cdot 6H_2O$, and Co $(NO_3)_2 \cdot 6H_2O$ in a mixture of isopropanol and DMAC. Then, the as-prepared NiCo-MOF material was transferred into an aqueous solution containing DMF ($V_{DMF}$: $V_{H2O}$ = 7: 1), subsequently Co $(NO_3)_2 \cdot 6H_2O$ and $NH_4H_2PO_4$ was added into the above solution under stirring. The decomposition of $NH_4H_2PO_4$ and the hydrolysis of DMF both produce hydroxyl groups, which promotes the coordination of $Co^{2+}$ and $(P_2O_7)^{4-}$ to form the final product NiCo-MOF/$Co_2P_2O_7$.

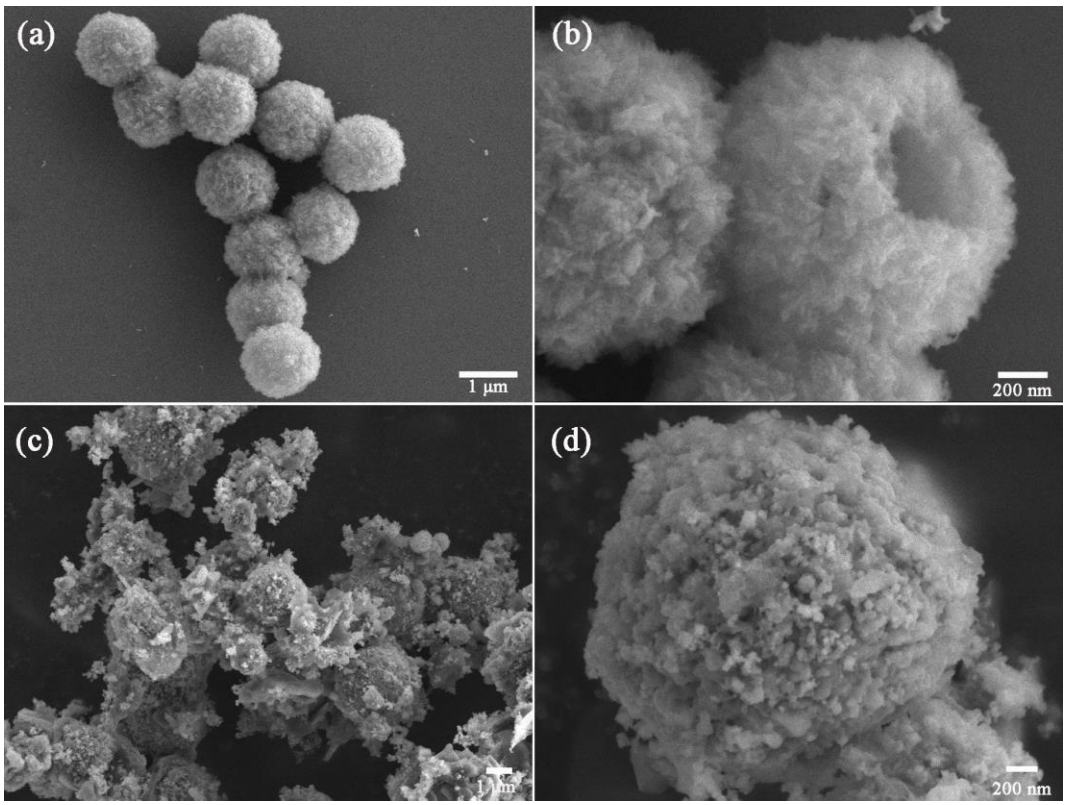


**Figure 1.** The typical SEM images of (a-b) NiCo-MOF and (c-d) NiCo-MOF/$Co_2P_2O_7$ at different magnifications.

The morphology and structure changes during the preparation was examined by electron microscopy. As shown in Figure 1a, NiCo-MOF exhibited a uniform and regular spherical morphology. Notably, from the Figure 1b with larger magnification, it is noted that, the spherical morphology is open, similar to a hollow bowl sphere which are assembled by ultrathin nanosheets, which is also confirmed in Figure S1. On the other hand, from Figure S2, it can be noticed that, the NiCo-MOF bowl-shaped sphere with a diameter of approximately 1.4 μm has a well-defined hollow morphology. After the phosphorylation treatment, the original hollow bowl-shaped sphere has a certain degree of destruction. Due to the formation of phosphorylated product, a large number of irregular particles are attached onto the surface to connect each other to form a porous structure (Figure 1c-d). Such a topographic structure is beneficial to increase the contact area between the electrolyte and the catalyst, expose more active sites, and ultimately enhance the electrocatalytic performance.

### *3.2. XRD analysis*

Figure 2 shows the X-ray diffraction (XRD) pattern which can disclose the crystal structure information of NiCo-MOF/$Co_2P_2O_7$. As shown in Figure 2a, the experimentally synthesized NiCo-MOF partially agrees well with the feature of the theoretically fitted Ni-MOF ([$Ni_2(OH)_2(C_8H_4O_4)$], CCDC No. 985792).[21] Specifically, the main peak of NiCo-MOF reflexes at 2θ positions of 9.02º, 14.28º, 15.98º and 18.00º, which is assigned to the (200), (001), (201), and (-201) crystalline planes of the Ni-

MOF, respectively. After phosphorylation, a series of new sharp diffraction peaks appeared at 16.76º, 23.84º, 29.06º, and 33.88º, corresponding to (011), (11-1), (120), and (031) crystal facets from the $Co_2P_2O_7$ (JCPDS No. 04-007-9045). For comparison, we also did the XRD test of monometallic pure Ni-MOF and pure Co-MOF after phosphorylation (Figure 2b). The results showed that their peaks are quite different, which means that the precursor is bimetallic NiCo which is more conducive to its phosphorylation.

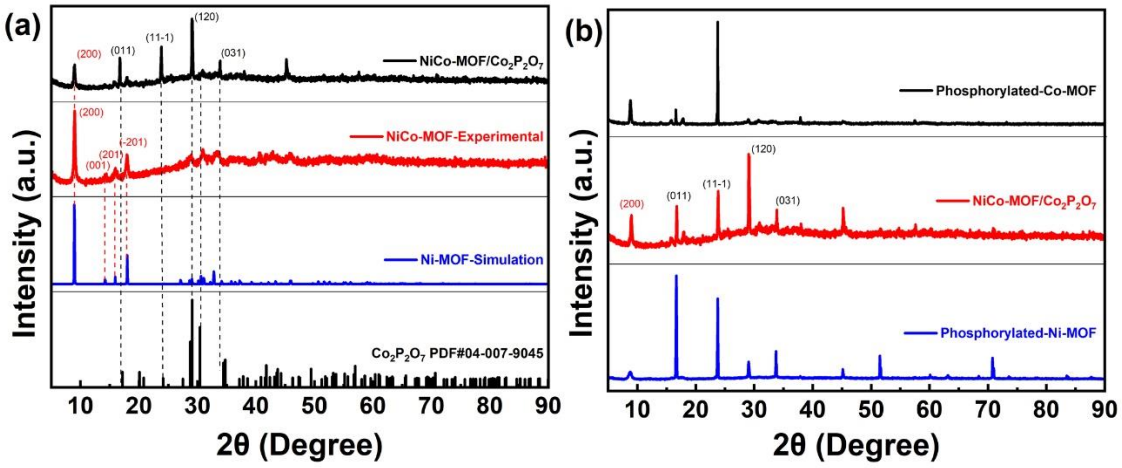


**Figure 2.** XRD patterns of (a) NiCo-MOF and NiCo-MOF/$Co_2P_2O_7$. (b) Phosphorylated Ni-MOF and Co-MOF.

### *3.3. OER performance of the phosphorylated NiCo-MOFs in alkaline media*

The electrocatalytic performance of NiCo-MOF/$Co_2P_2O_7$ toward OER in 1 M KOH was evaluated using the linear polarization curves. Firstly, we probed the influence of the Ni/Co ratios on the electrocatalytic performance of the NiCo-MOF. The results show that with the increase of the Ni/Co molar ratio (1: 0.5; 1: 1; 1: 2; 1: 3; 1: 4; 1: 5), the OER performance increased first and then decreased (Figure 3a). The NiCo-MOF with a 1: 3 Ni/Co ratio achieves the best performance, and the potential is 1.672 V at the current density of 50 mA $cm^{-2}$, the potential is 1.902 V @ 200 mA $cm^{-2}$. Note that, pure Ni-MOF has a slowly increasing broad peak after 1.40 V, which can be attributed to the oxidation peak of $Ni^{2+}$ to $Ni^{3+}$.

Then, we investigated the influence of the phosphide adding amount on the catalytic performance, and the mass ratios of the MOF and the phosphorus source were set to 1: 0.2, 1: 0.6, 1: 1, 1: 3,1: 5 (Figure 3b). The results show that the OER performance of the phosphating sample is significantly improved compared with the original NiCo-MOF materials. Among them, the sample with a mass ratio of 1:1 outperforms other samples in the series, whose overpotential is 408 mV at 50 mA $cm^{-2}$ and 583 mV at 200 mA $cm^{-2}$. We the compared the performance of the precursor NiCo-MOF, final product NiCo-MOF/$Co_2P_2O_7$ samples with commercial $RuO_2$. It can be clearly seen that, the performance of NiCo-MOF is comparable to $RuO_2$, while the performance of NiCo-MOF/$Co_2P_2O_7$ is far superior to $RuO_2$ (Figure 3c). The reaction kinetics was then analyzed using Tafel plots, and the Tafel

slope values can be obtained by fitting the linear portions according to the following equation: $\eta = blogj + a$, where $\eta$, $j$, $b$, and $a$ is the overpotential (V), current density (mA $cm^{-2}$), Tafel slope (mV $dec^{-1}$), and a constant, respectively. As displayed in Figure 3d, NiCo-MOF/$Co_2P_2O_7$ exhibited the lowest Tafel slope value of 106.4 mV $dec^{-1}$ compared with NiCo-MOF (151.8 mV $dec^{-1}$) and $RuO_2$ (187.6 mV $dec^{-1}$), which in good accordance with their catalytic activity.

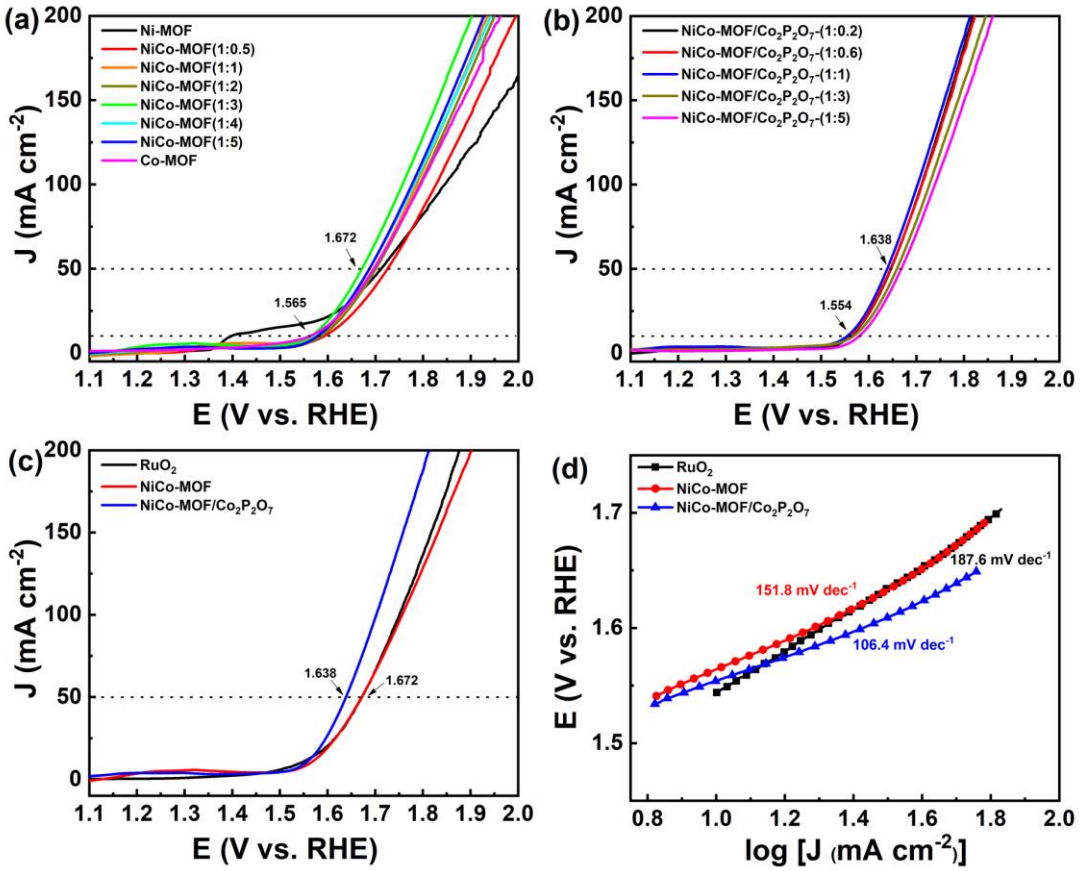


**Figure 3.** The linear sweep voltammetric curves of (a) NiCo-MOF with different Ni/Co ratios. (b) Different phosphorus-treated NiCo-MOF (Ni: Co=1: 3). (c) NiCo-MOF (1:3), NiCo-MOF/$Co_2P_2O_7$ (1:1) and commercial $RuO_2$. (d) Corresponding Tafel plots. The test was conducted in 1 M KOH with a scan rate of 10 mV $s^{-1}$.

### *3.4. Long term durability of NiCo-MOF/$Co_2P_2O_7$ with comparison of $RuO_2$ for OER*

Finally, chronoamperometric measurements were first conducted to evaluate the long-term durability of NiCo-MOF/$Co_2P_2O_7$ in comparison with $RuO_2$. As shown in Figure 4a, after continuous operation for 45, 000 s, the NiCo-MOF/$Co_2P_2O_7$ catalyst can retain 89.5% of its initial current value, while in stark contrast, $RuO_2$ only maintained 65.0% of the initial value at the same conditions. The higher current retention value indicates that NiCo-MOF/$Co_2P_2O_7$ has higher long-term durability than $RuO_2$. Furthermore, such robust stability of NiCo-MOF/$Co_2P_2O_7$ was further confirmed by the accelerated durability test by comparing the overpotential shift at a certain current density after 3000

cycles of potential scans. As shown in Figure 4b, after 3000 cycles of potential scan, the voltage value of NiCo-MOF/$Co_2P_2O_7$ had only a positive shift of only 24 mV, while the potential shift of $RuO_2$ is much larger (39 mV) (Figure 4c), further proving that NiCo-MOF/$Co_2P_2O_7$ had a markedly outperformed durability over the $RuO_2$ catalyst.

It is worth noting that, the OER performance of NiCo-MOF/$Co_2P_2O_7$ is also superior to most of the recently reported NiCo-based electrocatalysts with similar compositions or structures, as compiled in Table S1. For instance, in 1 M KOH for OER, at the current density of 10 mA $cm^{-2}$, even with smaller catalyst loading, the required overpotential of NiCo-MOF/$Co_2P_2O_7$ is 324 mV, smaller than that of CoNi-MOF (501 mV),[22] NNU-21 (550 mV),[23] Co-MOF-800 (520 mV),[24] $FeCo_2$-MOF (335 mV),[25] ZIF-67@$Co(OH)_2$ (354 mV),[26] 2D Co-BPDC/Co-BDC (335 mV),[27] and comparable with that of Ni–Co–Fe(NCF)-MOF (320 mV),[28] CoNi-Cu(BDC) (327 mV),[29] and $NiO_x$/$NiCo_2O_4$/$Co_3O_4$ (315 mV).[30] Such excellent OER performance can be mainly attributed to the fine porous structure of the NiCo-MOF, the synergistic effects of NiCo alloys, as well as the phosphorylation endowed enhancement.

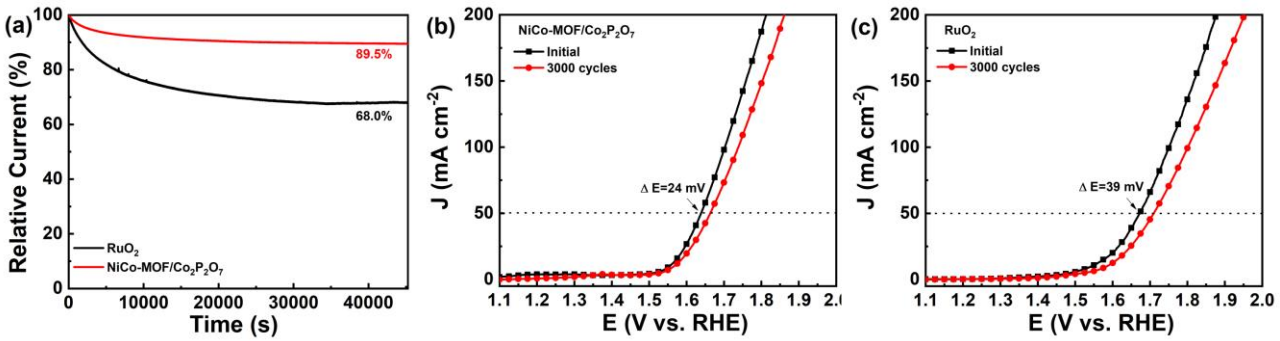


**Figure 4.** $RuO_2$ and NiCo-MOF/$Co_2P_2O_7$ (a) Chronoamperometric curves at 1.55 V for 45, 000 s. (b-c) The LSV curves before and post 3000 cycles of potential scan. The test was conducted in 1 M KOH with a scan rate of 10 mV $s^{-1}$.

## 4. CONCLUSIONS

In summary, the NiCo-MOF/$Co_2P_2O_7$ catalyst was synthesized after the hollow bowl-shaped MOF was phosphorylated by a mild two-step solvothermal method, which can serve as an excellent OER electrocatalyst. In alkaline medium, the NiCo-MOF/$Co_2P_2O_7$ (1: 1) catalyst exhibited the optimal electrocatalytic performance in the series, whose overpotential is 408 mV at 50 mA $cm^{-2}$ and 634 mV at 200 mA $cm^{-2}$. Moreover, the long term stability and durability surpass the benchmark $RuO_2$ catalyst. The remarkable electrocatalytic performance of NiCo-MOF/$Co_2P_2O_7$ can be attributed to the collaborative catalytic effects of the bimetallic NiCo and the contribution of phosphorylation to oxygen production. This study can pave the path for phosphorylated MOF based nanomaterials as an efficient OER catalyst toward sustainable energy storage and conversion.

SUPPLEMENTARY INFORMATION

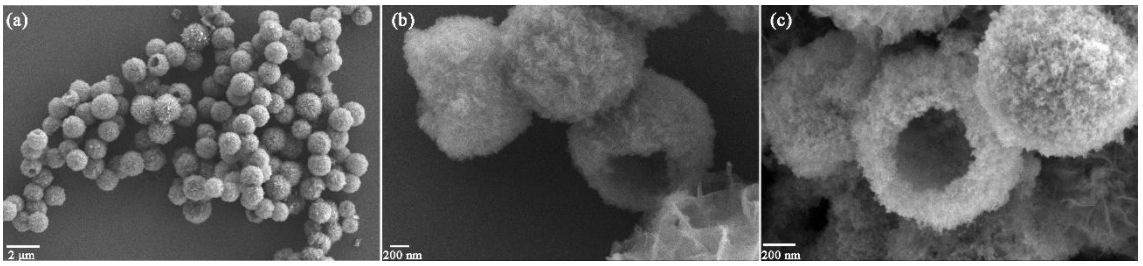


**Figure S1.** The typical SEM images of NiCo-MOF (1:3) at different magnifications.

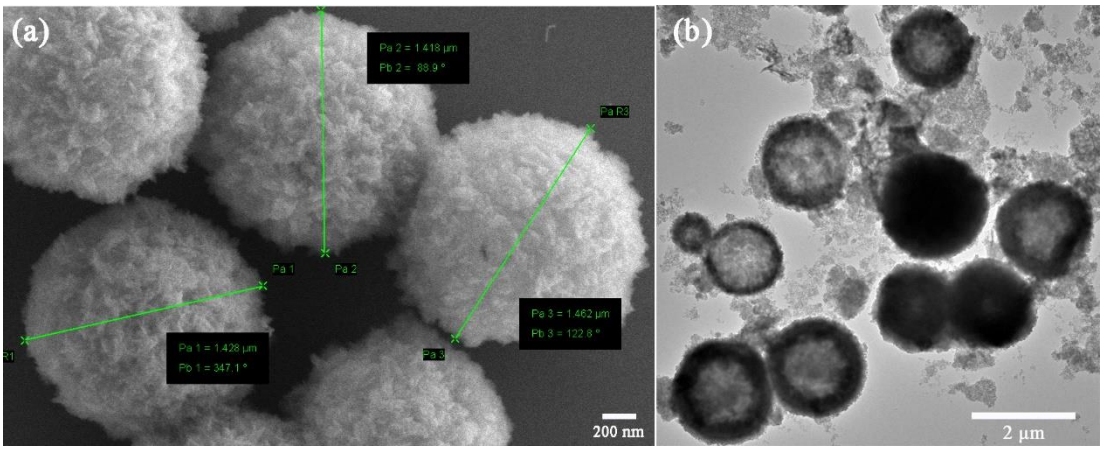


**Figure S2.** The typical SEM and TEM images of NiCo-MOF (1: 3).

**Table S1.** The OER performance comparison between $NiCo_{MOF}/Co_2(P_2O_7)$ and the recently reported NiCo-MOFs based electrocatalysts in 1 M KOH.

| Materials | Mass loading ($\mu g \cdot cm^{-2}$) | Current density ($mA \cdot cm^{-2}$) | η (mV) | Reference |
|---|---|---|---|---|
| **$NiCo_{MOF}/Co_2(P_2O_7)$** | 200 | 10 | 324 | **This work** |
| | | 50 | 409 | |
| | | 200 | 583 | |
| **Ni–Co–Fe (NCF)-MOF** | 200 | 10 | 320 | 28 |
| **CoNi-MOF** | 392 | 10 | 501 | 22 |
| **NNU-21** | 1000 | 10 | 550 | 23 |
| **Co-MOF-800** | 318 | 10 | 520 | 24 |
| **CoNi-Cu(BDC)** | 384 | 10 | 327 | 29 |
| **$FeCo_2$-MOF** | 566 | 10 | 335 | 25 |
| **ZIF-67@$Co(OH)_2$** | 200 | 10 | 354 | 26 |
| **2D Co-BPDC/Co-BDC** | 280 | 10 | 335 | 27 |
| **$NiO_x/NiCo_2O_4/Co_3O_4$** | - | 10 | 315 | 30 |

ACKNOWLEDGEMENTS
Z. M thanks the financial support from Chongqing Chemical Industry Vocational College.

**References**

1. L. Li, P. Wang, Q. Shao, X. Huang, *Chem. Soc. Rev.*, 49 (2020) 3072.
2. D. Li, Z. Zong, Z. Tang, Z. Liu, S. Chen, Y. Tian, X. Wang, *ACS Sustainable Chem. Eng.*, 6 (2018) 5105.
3. Y. Xu, W. Zhang, Y. Li, P. Lu, Z.-S. Wu, *J. Energy Chem.*, 43 (2020) 52.
4. L. C. Seitz, C. F. Dickens, K. Nishio, Y. Hikita, J. Montoya, A. Doyle, C. Kirk, A. Vojvodic, H. Y. Hwang, J. K. Norskov, T. F. Jaramillo, *Science,* 353 (2016) 1011.
5. Z.-P. Wu, X. F. Lu, S.-Q. Zang, X. W. Lou, *Adv. Funct. Mater.,* 30 (2020) 1910274.
6. C. Tsounis, X. Lu, N. M. Bedford, B. Subhash, L. Thomsen, Q. Zhang, Z. Ma, K. Ostrikov, A. Bendavid, J. A. Scott, R. Amal, Z. Han, *ACS Nano,* 14 (2020) 11327.
7. W. Xu, M. Andersen, K. Reuter, *ACS Catal.,* 11 (2021) 734.
8. X. Han, X. Wu, C. Zhong, Y. Deng, N. Zhao, W. Hu, *Nano Energy,* 31 (2017) 541.
9. Z. Qian, Y. Chen, Z. Tang, Z. Liu, X. Wang, Y. Tian, W. Gao, *Nano-Micro Lett.*, 11 (2019) 28.
10. B. Qiu, L. Cai, Y. Wang, Z. Lin, Y. Zuo, M. Wang, Y. Chai, *Adv. Funct. Mater.*, 28 (2018) 1706008.
11. H. Xu, J. Cao, C. Shan, B. Wang, P. Xi, W. Liu, Y. Tang, *Angew. Chem., Int. Ed.*, 57 (2018) 8654.
12. Z. Fu, S. Liu, Z. Mai, Z. Tang, D.-D. Qin, Y. Tian, X. Wang, *Chem. Asian J.*, 15 (2020) 3568.
13. X. F. Lu, B. Y. Xia, S.-Q. Zang, X. W. Lou, *Angew. Chem. Int. Ed.*, 59 (2020) 4634.
14. L. Jiao, H.-L. Jiang, *Chem*, 5 (2019) 786.
15. H.-F. Wang, L. Chen, H. Pang, S. Kaskel, Q. Xu, *Chem. Soc. Rev.,* 49 (2020) 1414.
16. W. Wang, X. Xu, W. Zhou, Z. Shao, *Adv. Sci.*, 4 (2017) 1600371.
17. Z. Xue, K. Liu, Q. Liu, Y. Li, M. Li, C.-Y. Su, N. Ogiwara, H. Kobayashi, H. Kitagawa, M. Liu, G. Li, *Nat. Commun.*, 10 (2019) 5048.
18. Q. Ji, Y. Kong, C. Wang, H. Tan, H. Duan, W. Hu, G. Li, Y. Lu, N. Li, Y. Wang, J. Tian, Z. Qi, Z. Sun, F. Hu, W. Yan, *ACS Catal.*, 10 (2020) 5691.
19. C. Li, X.-J. Li, Z.-Y. Zhao, F.-L. Li, J.-Y. Xue, Z. Niu, H.-W. Gu, P. Braunstein, J.-P. Lang, *Nanoscale*, 12 (2020) 14004.
20. L. Xiao, Q. Zhao, L. Jia, Q. Chen, J. Jiang, Q. Yu, *Electrochim. Acta*, 304 (2019) 456.
21. A. Mesbah, P. Rabu, R. Sibille, S. Lebègue, T. Mazet, B. Malaman, M. François, *Inorg. Chem.*, 53 (2014) 872.
22. C. Yang, W.-J. Cai, B.-B. Yu, H. Qiu, M.-L. Li, L.-W. Zhu, Z. Yan, L. Hou, Y.-Y. Wang, *Catal. Sci. Technol.*, 10 (2020) 3897.
23. X.-L. Wang, L.-Z. Dong, M. Qiao, Y.-J. Tang, J. Liu, Y. Li, S.-L. Li, J.-X. Su, Y.-Q. Lan, *Angew. Chem., Int. Ed.*, 57 (2018) 9660.
24. X. Duan, N. Pan, C. Sun, K. Zhang, X. Zhu, M. Zhang, L. Song, H. Zheng, *J. Energy Chem.*, 56 (2021) 290.
25. M. Gu, S.-C. Wang, C. Chen, D. Xiong, F.-Y. Yi, *Inorg. Chem.*, 59 (2020) 6078.
26. J.-F. Qin, J.-Y. Xie, N. Wang, B. Dong, T.-S. Chen, Z.-Y. Lin, Z.-Z. Liu, Y.-N. Zhou, M. Yang, Y.-M. Chai, *J. Colloid Interf. Sc.*, 562 (2020) 279.
27. Q. Zha, F. Yuan, G. Qin, Y. Ni, *Inorg. Chem.*, 59 (2020) 1295.
28. W. Ahn, M. G. Park, D. U. Lee, M. H. Seo, G. Jiang, Z. P. Cano, F. M. Hassan, Z. Chen, *Adv. Funct. Mater.*, 28 (2018) 1802129.
29. J. Ma, B. Lu, S. Wang, W. He, X. Bai, T. Wang, X. Zhang, Y. Li, L. Zhang, J. Chen, F. Meng, Y. Fu, *New J. Chem.*, 44 (2020) 2459.

30. J. Chen, Y. Ling, Z. Lu, X. Huai, F. Qin, Z. Zhang, *Electrochim. Acta,* 322 (2019) 134753.